Electronic Supplementary Material (ESI) for ChemComm.
This journal is © The Royal Society of Chemistry 2017

Supplementary Material for

Robust superhydrophobic diamond microspheres for no-loss transport of corrosive liquid microdroplets

Qiang Wang, Jie Bai, Bing Dai, Zhenhuai Yang, Shuai Guo, Lei Yang and Jiaqi Zhu*

*Corresponding author. E-mail: zhujq@hit.edu.cn

This file includes:
Materials and Methods
Supplementary Figures and Text
Figs. S1 to S11

Materials and Methods

Materials

Aqueous nanodiamond solution were purchased from ZhongNan Diamond Co., Ltd, and the size of nanodiamond in the solution is around 10-30 nm. Silicon wafers (2 inches in size), glass slides, and disposable syringes were purchased from Aladdin Industrial Inc.. Hydrochloric acid, sodium hydroxide, acetone and ethanol were purchased from Beijing Chemical works. Deionized water was purchased from Harbin BaiDa Industrial Inc., and used for all experiments. The test corrosive liquids with pH varied from 1 to 14 were prepared by using titration to discover the concentrations of solutions of hydrochloric acid and sodium hydroxide, and the pH values were determined by pH test paper. Commercial epoxy glue (Henkel Pattex PKM12C-1) was purchased from Henkel (China) Investment Co., Ltd., and the main component of the product is epoxy. N_2 (99.9%), H_2 (99.999%), and CH_4 (99.999%) were purchased from Harbin Liming Co., Ltd.

Diamond microsphere preparation

First of all, the silicon wafer was cleaned by acetone, ethanol and deionized water respectively, and dried by N_2. Afterwards, the aqueous nanodiamond solution was evenly dispersed on surface of the cleaned silicon wafer by spin-coating process. The optical image of the aqueous nanodiamond solution and the TEM images of the nanodiamond seeds are shown in Fig. S1. It reveals that the aqueous nanodiamond solution won't be settling and the nanodiamond seeds are fully spread out with a size around 10-30 nm. Then, the silicon wafer coated by nanodiamond seeds was put in the vacuum chamber of microwave-plasma-assisted chemical vapor deposition (MPACVD) system. The substrate was directly heated by being immersed in plasma; no other heating source was used. The surface temperature of the sample was measured by infrared temperature measurement system. The power of 3000 W and a ratio of 80/20 sccm for H_2/CH_4 at the temperature/pressure of 550 °C/85 mbar were used to grow diamond microspheres on the silicon wafer.

Characterizations

Surface morphology of specimens was examined by a scanning electron microscope (SEM, FEI Helios Nanolab 660i, operated at 5-20 kV). The morphology and micro-structure of the samples were studied in detail by transmission electron microscope (TEM, FEI Tecnai G2 F30, operated at 300 kV). Raman spectra were acquired on a confocal Raman spectroscope (Horiba Jobin-Yvon Lab RAM HR800 System) with 458 nm laser excitation under ambient conditions. The structure of as-perpared diamond microspheres was studied using a grazing incidence X-ray diffractometer (GIXRD, PANalytical X' Pert Pro Cu Kα). Water contact angles (CA) were measured on an OCA20 system (Data-Physics) under ambient conditions; and the size of the water droplets was 5 μl. The CA values are the averages with corresponding standard deviation that were measured at five different areas on each sample. Optical microscopy images were taken on a Nikon D7100.

Supplementary Figures and Text

Nano-diamond seeds

Fig. S1 shows the optical image the aqueous nanodiamond solution; and the TEM images of the nanodiamond seeds. In this figure, the size of the nanodiamond seeds is around 10-30 nm; and they are fully spread out.

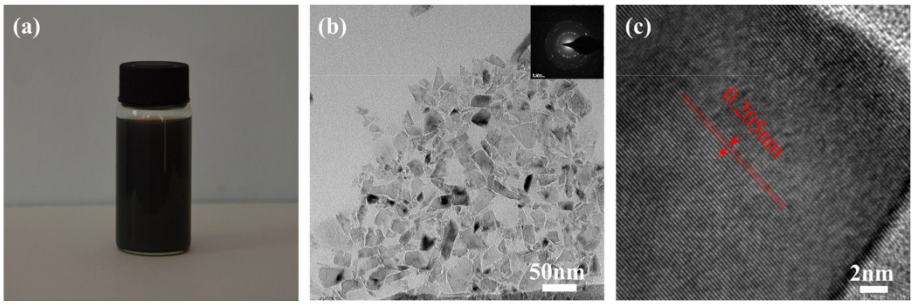

Fig. S1.
(a) Optical image of the aqueous nanodiamond solution. (b) TEM image and SAED pattern of the nanodiamond seeds. (c) HRTEM image of a nanodiamond seeds.

The contact angle of as-prepared diamond microspheres

The diamond microspheres were directly synthesized on the surface of silicon wafers (2 inches in size). The water contact angle of as-prepared diamond microspheres is about 161° as shown in Fig. S2.

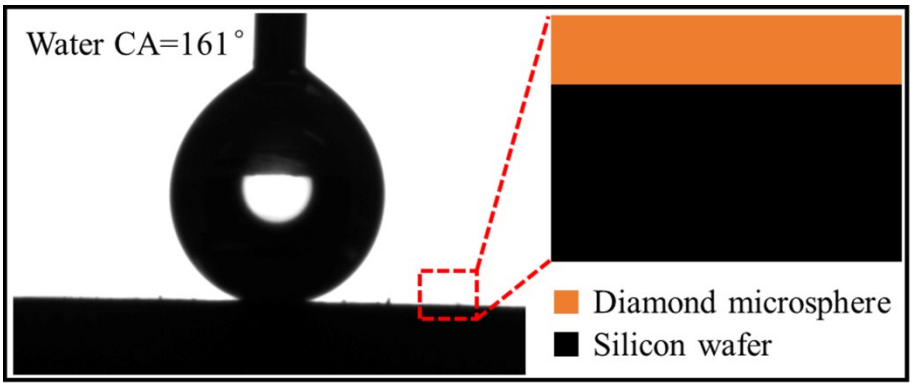

Fig. S2.
The water contact angle of as-prepared diamond microspheres. It was measured on an OCA20 system (Data-Physics) under ambient conditions; and the water droplets was 5 µl.

<u>The sliding angle of as-prepared diamond microspheres</u>

Owing to the multilevel hierarchical structure formed and the large volume of air trapped beneath the water droplet, the Cassie state was created. Further, given that the fabricated microspheres constituted a composite powder with good flowability, the water droplets readily rolled off the surface during the dispensing process; this was the case even when the sample was placed on a horizontal plane, as shown in Fig. S3. This indicated that the sliding angle is close to 0° and the adhesive force is ultralow, thus ensuring that the water droplets could readily roll off the surface.

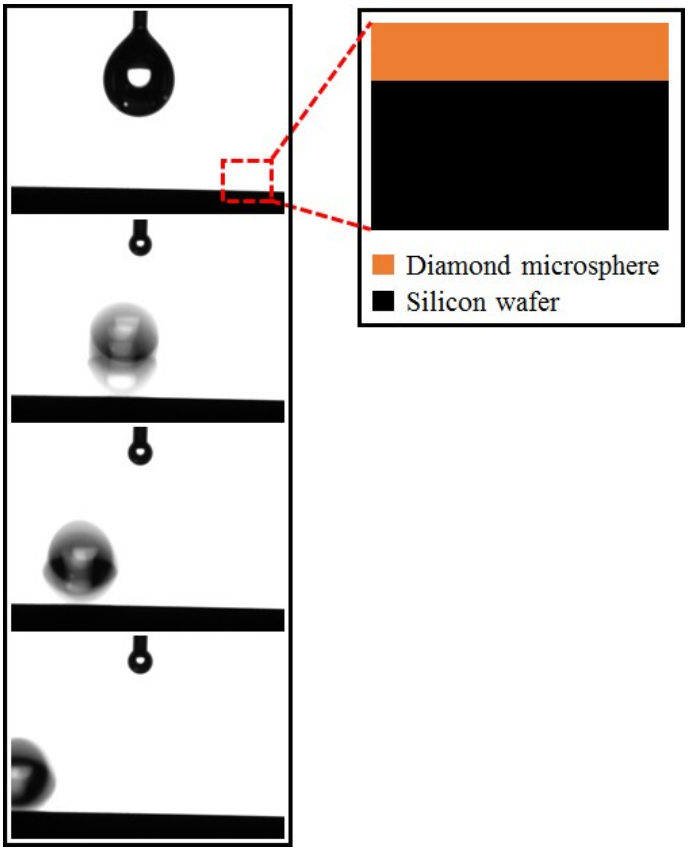

Fig. S3.

The water sliding angle of as-prepared diamond microspheres; successive images of the dynamic movement of a water droplet (10 μl) on a typical sample placed on a horizontal plane.

The method of collecting the diamond microspheres

The as-grown diamond microspheres are similar to agglomerated nano-diamond

powder, and they can be readily scratched by a blade from Si substrate and then collected together or transferred to other substrates. The cross-sectional image of the diamond microspheres synthesized on Si substrate is shown in Fig. S4.

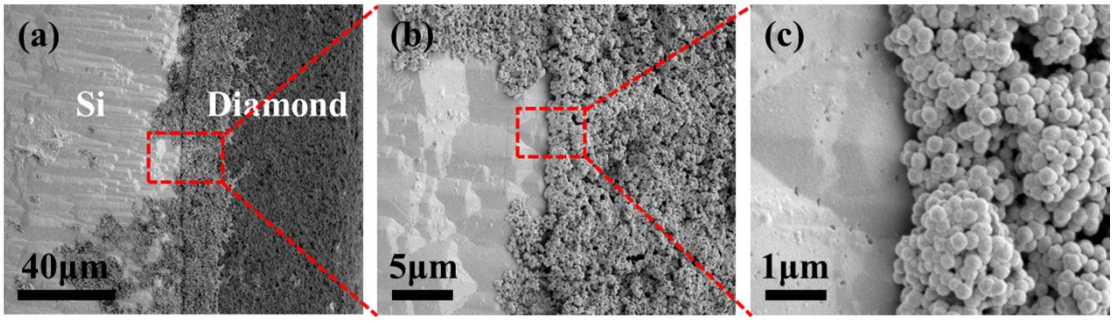

Fig. S4.

(a) Cross-sectional SEM image of the diamond microspheres synthesized on Si substrate. (b) Magnified SEM image. (c) Further magnified SEM image.

The as-grown diamond microspheres scratched from a Si substrate is shown in Fig. S5. It shows that the collected diamond microspheres resemble nano-diamond powder, and they can be readily transferred to other substrates.

Fig. S5.

Optical image of the diamond microspheres scratched from a Si substrate.

<u>The preparation procedure of the composite film</u>

The as-grown diamond microspheres were directly transferred to various material

surfaces with fixing them with commercial epoxy glue. The detailed preparation procedure of the composite film coated on glass slide as an example is shown in Fig. S6. The epoxy glue was cured sufficiently so that the microspheres were firmly fixed on the surface. The extra microspheres not adhered to the surface were collected by a brush, and finally cleaned by N_2 at a pressure of 0.4 MPa. The obtained composite film shows robust superhydrophobicity and ultrahigh adhesive force.

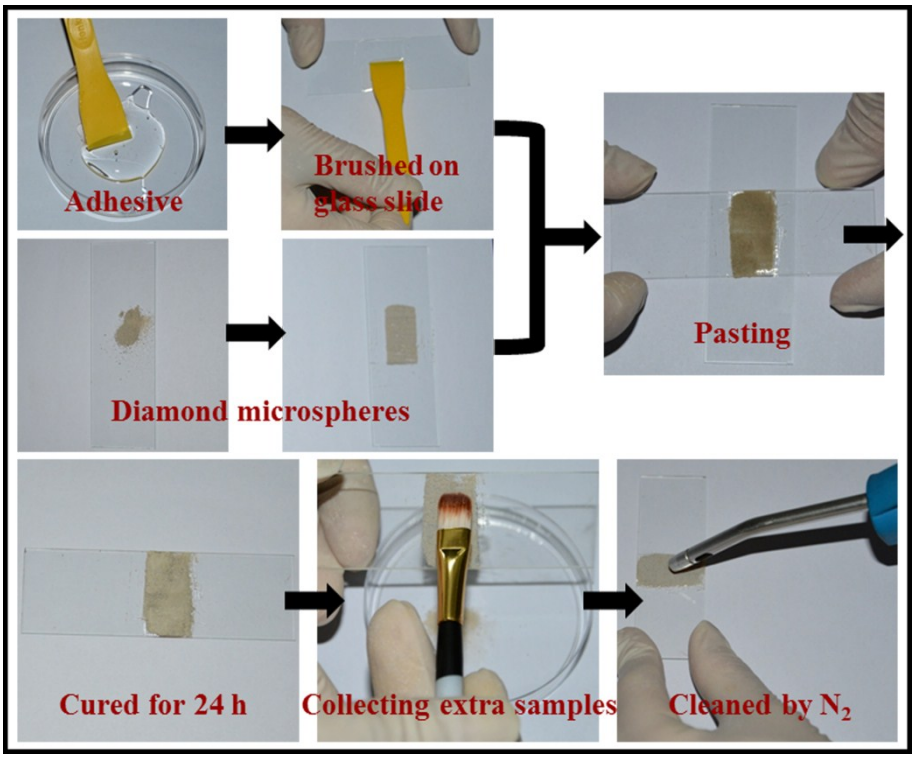

Fig. S6.

Flow diagram for the fabrication of the composite film. The obtained composite film shows robust superhydrophobicity and ultrahigh adhesive force.

<u>The characterizations of the cured epoxy glue film</u>

The epoxy glue was brushed on glass slides and cured sufficiently under ambient

conditions for 24 h. The topography and roughness of the cured adhesive were measured by AFM as shown in Fig. S7a. It reveals that the cured adhesive is quite smooth, and the roughness is about 0.25nm. The contact angles of the cured adhesive were measured by dropping a droplet (5 μl, deionized water or corrosive liquid) on top of the surfaces. As shown in Fig. S7(b-d), the contact angles of the cured epoxy glue film are about 30°, and shows obvious hydrophilicity. In addition, the resistance to the corrosive liquid of the cured epoxy glue film was investigated by immersing the cured films in 2M HCl and 2M NaOH solutions for 240 hours, respectively. Fig. S7(e-g) show that the surface topographies of the films were nearly unchanged after being immersed in the corrosive liquid.

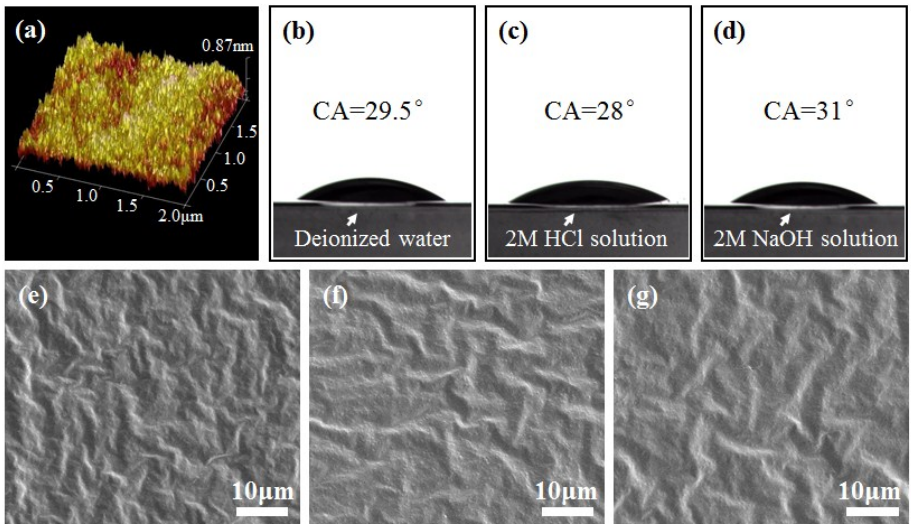

Fig. S7.

(a) AFM image of the cured epoxy glue film. (b)-(c) Contact angles of the cured films. (e) SEM image of the cured film. (f) SEM image of the film immersed in 2M HCl solution for 240 hours. (g) SEM image of the film immersed in 2M NaOH solution for 240 hours.

The wettability properties of the composite films

Fig. S8 show the optical images of as-prepared diamond microspheres coated on top of a glass slide. The contact angle for the pure water (PH=7) is about 158° (Fig. S8a); and

the adhesive force is so high that the water droplet (5 μL) can't roll any more under the various angles of the tilt, even when the tilt angle is 180°, as shown in Fig. S8(b-d).

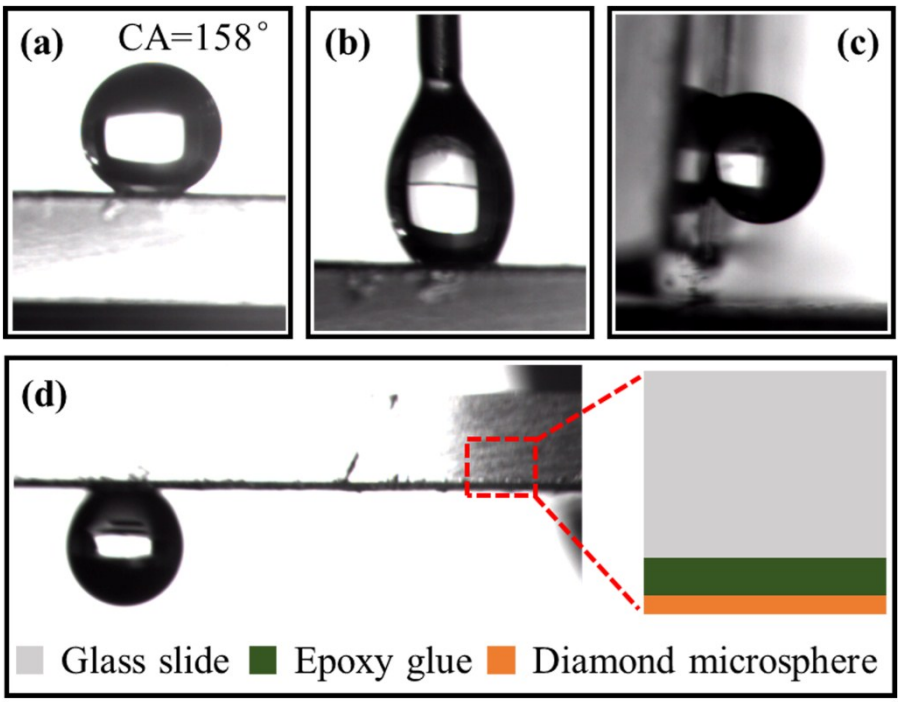

Fig. S8.
(a) The water contact angle of the composite film. (b) Optical image of a water droplet directionally transferred from the untreated syringe needle to the composite surface. The water droplet (5 μl) can't roll any more under the various angles of the tilt; (c) the tilt angle is 90° and (d) the tilt angle is 180°.

No-loss transport of liquid droplets

Fig. S9 shows that the composite film continued to exhibit superhydrophobicity and a high adhesive force in the case of water droplets with different pH values. It can be used for the applications as no-loss transport of liquid droplets, even for the liquid droplets with

strong corrosivity. The sizes of the water droplets are all 10 μl, and the PH value of the water droplet is 2 in Fig. S9a, 7 in Fig. S9b, and 12 in Fig. S9c.

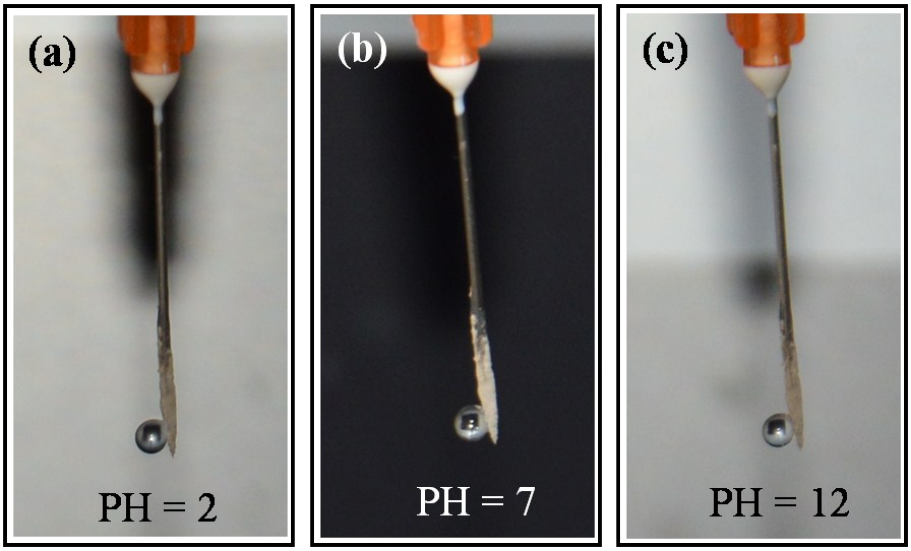

Fig. S9.
Optical images of using the syringe needle coated the as-prepared composite film for no-loss transport of water droplets. (a) The water PH value is 2. (b) The water PH value is 7. (c) The water PH value is 12.

The dynamic movement of dispensing a water droplet to the composite film

Owing to the difference in the adhesive forces, a water micro-droplet (5 μL) could be directionally dispensed from the untreated needle to the composite film (Fig. S10). Then, the composite film could be acted as a "mechanical hand" to transfer the micro-droplet to

a hydrophilic surface without any weight loss or contamination. It is useful for a wide range of applications, such as localized chemical or biological reactions, traced analysis, and in situ detection.

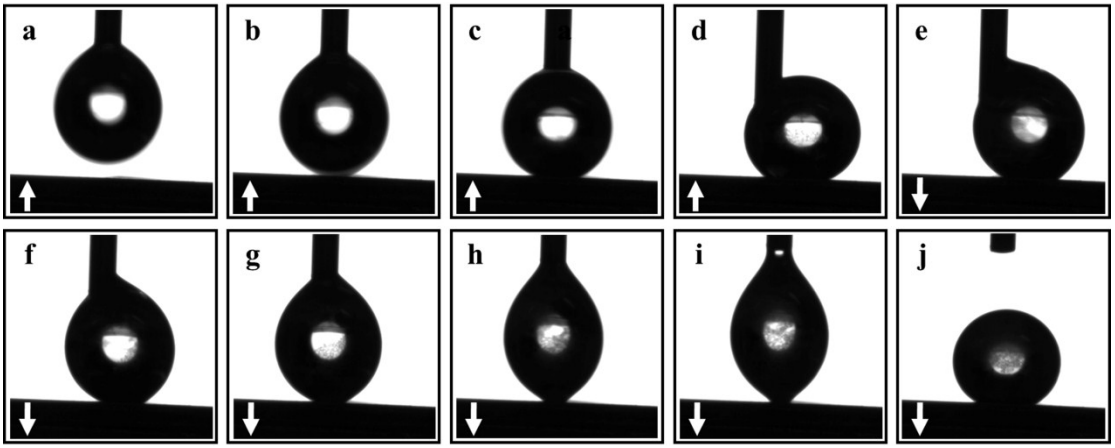

Fig. S10.
Successive images of the dynamic movement of no-loss transport of a water droplet. A water droplet (5 μl) is directionally transferred from untreated syringe needle to the as-prepared composite surface. (a)-(d) The composite surface approaches, touches, and presses the water droplet hanging on the top of a syringe needle. (e)-(j) The composite surface releases and catches the water droplet, and leaves the syringe needle.

Sandpaper abrasion and knife-scratch tests

A steel substrate (with a semidiameter of 1 cm) coated by the as-prepared composite film was used as one example for sandpaper abrasion and knife-scratch tests. The

composite film was directionally (10 cm for a cycle) abraded by the sandpaper (Standard glasspaper, Germany Matador P320) under a weight at 20 g. Fig. S11a shows that the steel substrate is still superhydrophobic after sandpaper abrasion test for 10 cycles; the water contact angle is about 143°. Then, the steel substrate continued to be used for knife-scratch test. Fig. S11b shows that the test sample still kept superhydrophobicity after being subjected to the multiple abrasion cycles using sandpaper and knife-scratch test, and the contact angle is about 141°. These tests indicated that the synthesized composite surface shows desirable mechanical property.

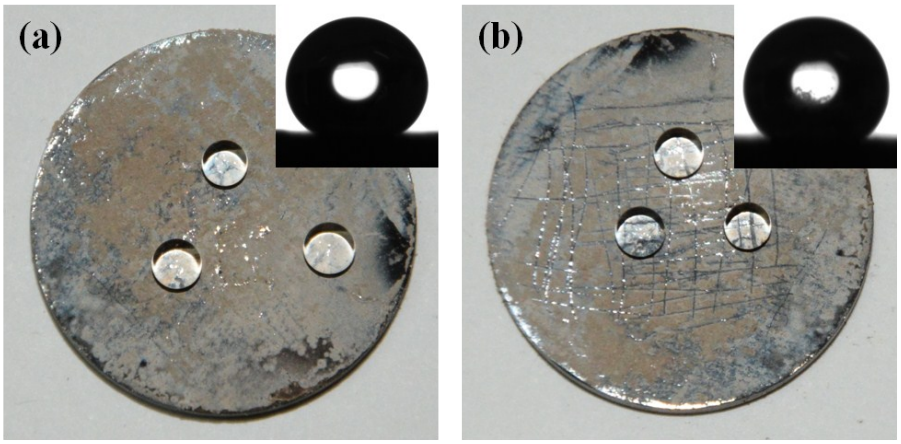

Fig. S11.

(a) Optical image and the water contact angle of the steel substrate after sandpaper abrasion test for 10 cycles. (b) Optical image and the water contact angle of the steel substrate after being subjected to the multiple abrasion cycles using sandpaper and knife-scratch test.

Table S1 Peaks of different structural carbons in Raman spectra of CVD nanodiamond[1-6]

Raman shift (cm^{-1})	Assignment

1100～1150	Trans-polyacetylene on grain boundary or disordered sp^3 carbon
1230～1280	Maximum in the diamond vibrational density of states
1332	Diamond
1350	Sp^2 carbon (D mode)
1430～1470	Trans-polyacetylene on grain boundary
1520～1580	Sp^2 carbon (G mode)

References

1 Prawer S, Hoffman A, Stuart S A, et al. Correlation between crystalline perfection and film purity for chemically vapor deposited diamond thin films grown on fused quartz substrates. Journal of applied physics, 1991, 69(9): 6625-6631.

2 Buckley R G, Moustakas T D, Ye L, et al. Characterization of filament‐assisted chemical vapor deposition diamond films using Raman spectroscopy. Journal of Applied Physics, 1989, 66(8): 3595-3599.

3 Nistor L C, Van Landuyt J, Ralchenko V G, et al. Nanocrystalline diamond films: transmission electron microscopy and Raman spectroscopy characterization. Diamond and Related Materials, 1997, 6(1): 159-168.

4 Ferrari A C, Robertson J. Origin of the 1150 cm^{-1} Raman mode in nanocrystalline diamond. Physical Review B, 2001, 63(12): 121405.

5 Wang Y, Alsmeyer D C, McCreery R L. Raman spectroscopy of carbon materials: structural basis of observed spectra. Chemistry of Materials, 1990, 2(5): 557-563.

6 Ferrari A C, Robertson J. Raman spectroscopy of amorphous, nanostructured, diamond–like carbon, and nanodiamond. Philosophical Transactions of the Royal Society of London A: Mathematical, Physical and Engineering Sciences, 2004, 362(1824): 2477-2512.